Transcriptome analysis of hydrogen inhibits osteoclastogenesis of mouse bone marrow mononuclear cells

YONG LIU[1*], WEI WANG[2*], YONG ZENG[1] and HUI ZENG[3]

[1]Department of Orthopedics, Chengdu Second People's Hospital, Chengdu, Sichuan 610017; [2]Department of Human Anatomy and Histoembryology, Zhuhai Campus of Zunyi Medical University, Zhuhai, Guangdong 519041; [3]Department of Bone and Joint Surgery, Peking University Shenzhen Hospital, Shenzhen, Guangdong 518036, P.R. China

Received April 10, 2022; Accepted September 1, 2022

DOI: 10.3892/etm.2023.12135

Abstract. Hydrogen (H_2) is a major biodegradation product of implanted magnesium (Mg) alloys that are commonly used in the healing of bone fractures. Our earlier study showed that H_2 can inhibit mouse bone marrow mononuclear cell (BMMC) osteoclastogenesis during the differentiation of these cells into osteoclasts, thereby facilitating fracture healing. However, the way by which H_2 inhibits osteoclastogenesis remains to be elucidated. The present study used RNA-sequencing to study the transcriptome of H_2-exposed BMMCs in an osteoclast-induced environment and identified the target genes and signaling pathways through which H_2 exerts its biological effects. Several upregulated genes were identified: *Fos*, *Dusp1*, *Cxcl1*, *Reln*, *Itga2b*, *Plin2*, *Lif*, *Thbs1*, *Vegfa* and *Gadd45a*. Several downregulated genes were also revealed: *Hspa1b*, *Gm4951*, *F830016B08Rik*, *Fads2*, *Hspa1a*, *Slc27a6*, *Cacna1b*, *Scd2*, *Lama3* and *Col4a5*. These differentially expressed genes were mainly involved in osteoclast differentiation cascades, as well as PI3K-AKT, Forkhead box O (FoxO), MAPK, peroxisome proliferator-activated receptor (PPAR), TNF, TGF-β, JAK-STAT, RAS, VEGF, hypoxia-inducible factor (HIF-1) and AMPK signaling pathways. In summary, the present study revealed the key genes and signaling pathways involved in the H_2-mediated inhibition of osteoclastogenesis, thereby providing a theoretical basis for the significance of H_2 and an experimental basis for the application of Mg alloys in the treatment of osteoporosis.

Correspondence to: Dr Yong Liu, Department of Orthopedics, Chengdu Second People's Hospital, 10 Qingyun South Street, Chengdu, Sichuan 610017, P.R. China
E-mail: dragonliu999@126.com

Professor Hui Zeng, Department of Bone and Joint Surgery, Peking University Shenzhen Hospital, 1120 Lianhua Road, Shenzhen, Guangdong 518036, P.R. China
E-mail: zenghui_36@pkuszh.com

*Contributed equally

Key words: magnesium, hydrogen, bone marrow mononuclear cell, osteoclastogenesis, RNA-sequencing

Introduction

Magnesium (Mg), as well as its alloys, is a new type of biodegradable metallic material used in bone repair and regeneration (1). Compared with the currently approved metallic agents, such as titanium and stainless steel, Mg alloys possess improved osteo-inductive and osteo-conductive capacities, well adapted for bone healing *in vivo* and *in vitro* (2-4), hence Mg alloys are of great interest for orthopedic applications (5). One of the degradation products of Mg alloy implants *in vivo*, H_2, is a physiologically inert gas. A previous study demonstrated that H_2 has a variety of physiological functions and therapeutic effects, which have been studied in ~166 human disease models thus far (6). For musculoskeletal applications, the results of animal experiments have revealed that H_2 can alleviate bone loss caused by microgravity (7,8) and that H_2-rich water can inhibit the resorption of alveolar bone (9).

Osteoclasts originate from bone marrow mononuclear cells (BMMCs), which are derived from hematopoietic stem cells and they can differentiate into osteoclasts *in vitro* through Rankl-induced NF-κB, MAPK and AKT signaling pathways (10,11). These highly specialized cells can degrade and digest the bone matrix (12-14). Furthermore, the aberrant production and/or the abnormal lifespan of osteoclasts have been found to be the cause(s) of benign or malignant bone diseases (15,16). As such, osteoclasts have important roles in bone formation and remodeling (17).

Our previous study revealed that H_2 can inhibit BMMC osteoclastogenesis in mice (18). It was observed that treatment with 50% H_2 for 7 days could inhibit osteoclast formation, osteoclast function and osteoclast-related gene expression of osteoclast-induced BMMCs and that treatment with 50% H_2 could reduce proliferation, promote apoptosis and inhibit the expression of osteoclast-related proteins in BMMCs cultured in osteoclast-induced medium.

Briefly, in pit formation assays, there was no difference among the three groups (25, 50 and 75% H_2) when exposed to this inert gas for 5, 7 or 10 days. In reverse transcription-quantitative (RT-q) PCR analyses, when BMMCs were treated

with H_2 for 5 days, the expression of the three osteoclast-related genes could not be inhibited. When BMMCs were induced for 7 or 10 days, treatment with 2% H_2 had no inhibitory effect on the expression of osteoclast-related genes, while treatment with 25, 50, or 75% H_2 (especially 50 and 75% H_2) significantly reduced the expression levels of the osteoclast-related genes *Ctsk*, *Calcr* and *Mmp9*. Therefore, based on these findings and the results of a previous study (19), treatment with 50% H_2 for 7 days was selected as the optimal condition to investigate the role of H_2 in BMMC proliferation and apoptosis. However, the mechanism by which this occurs, which is critical for the translational research of H_2 and Mg alloys and the treatment of osteoporosis, remains to be elucidated. The present study used transcriptome sequencing to identify the possible mechanism behind the H_2-mediated inhibition of osteoclastogenesis and revealed the key genes and signaling pathways involved, thereby providing a theoretical basis for the anti-osteoporosis function of H_2.

Materials and methods

BMMC culture and osteoclast induction. BMMCs were isolated as previously reported (20,21). In brief, four-week-old C57BL/6 mice (~20 g) were purchased (Changzhou Cavens Laboratory Animal Co., Ltd.). After the animals (3 weeks old) were received, adaptive feeding was performed for 1 week. Food and water were freely available throughout the experiment. The animals were maintained at 20-25˚C, with a 12:12 h light and dark cycle and a relative humidity of 45-60%. When the animals were 4 weeks old, they were sacrificed by neck-dislocation and disinfected with 75% alcohol. Under sterile conditions, the bilateral femurs and tibias were removed. The metaphyses of the long bones were obtained and the bone marrow cavities were gently and repeatedly irrigated with serum-free α-minimum essential medium (α-MEM; HyClone; Cytiva). The collected washes were filtered through a 200-mesh sieve and centrifuged (Sigma 3K15; Sigma Laborzentrifugen GmbH) at 232 x g for 5 min at 20˚C. The supernatant was discarded and the pelleted cells were resuspended in sterile BL503A erythrocyte medium (Biosharp Life Sciences), gently mixed by inversion and lysed on ice for 5 min. Subsequently, the cell suspension was centrifuged at 161 x g for 5 min at 20˚C. and the supernatant containing the lysed red blood cells was discarded. The pelleted cells were resuspended, washed twice in serum-free α-MEM and resuspended in 3 ml of α-MEM containing 10% fetal bovine serum (FBS; Gibco; Thermo Fisher Scientific, Inc.). The cells were statically inoculated in 60-mm culture dishes and incubated overnight in a humidified atmosphere of 5% CO_2 at 37˚C. Thereafter, the supernatant was collected and centrifuged at 232 x g for 3 min at 20˚C to obtain the mouse BMMCs. The BMMCs were resuspended in α-MEM containing 10% FBS, appropriately diluted and inoculated in 3.5 cm diameter culture dishes at ~$1x10^5$ primary cells per well. The medium was replaced every two days.

Depending on the H_2 concentration in the incubator, the primary cells (P1) were divided into two groups as follows: The experimental group (BMMCs + 50% H_2 + 20% O_2 + 5% CO_2 + 25% N_2) and the control group (BMMCs + 20% O_2 + 5% CO_2 + 75% N_2). The H_2 in the incubator entered the cell culture medium by dissolution-diffusion. To induce osteoclast differentiation, 20 ng/ml macrophage colony stimulating factor (Csf1; PeproTech China) and 50 ng/ml receptor activator of NF-κB ligand (Rankl; R&D Systems, Inc.) were used. The BMMCs were cultured in separate incubators at 37˚C with or without 50% H_2 as aforementioned for 7 days and six repetitions were tested for each treatment group. Therefore, a total of 12 samples were collected; and six C57BL/6 mice, half male and half female, were used in this experiment.

Ethics statement. The present study was conducted in accordance with the ethical standards of the Ethics Committee of Peking University Shenzhen Hospital, who approved the experimental protocols.

Total RNA extraction. Total RNA was extracted from the cells using TRIzol® (Thermo Fisher Scientific, Inc.), according to the manufacturer's instructions. In brief, 1.5 ml of TRIzol® was added to the pelleted cells, followed homogenization for 2 min and a 5-min horizontal rest period to permit the complete dissociation of nucleoprotein complexes. The mix was centrifuged at 12,000 x g for 5 min at 4˚C. The upper phase was transferred into new tubes and 0.3 ml of chloroform/isoamyl alcohol (24:1) was added. The samples were vortexed and centrifuged at 12,000 x g for 10 min at 4˚C. Thereafter, the upper aqueous phase was transferred into a new tube and an equivalent volume of isopropyl alcohol (Xilong Science Co., Ltd.) was added, followed by vortexing, precipitation and centrifuged at 17,500 x g for 20 min at 4˚C. The pelleted RNA was washed twice with 75% ethanol, air-dried and resuspended in 25 μl of diethyl pyrocarbonate-treated water. The RNA was qualified and quantified using an Agilent 2100 bioanalyzer (Agilent Technologies, Inc.) and a Nanodrop spectrophotometer (Thermo Fisher Scientific, Inc.), respectively.

mRNA library construction. mRNA library construction and transcriptome sequencing were performed at the Beijing Genomics Institution (Fig. 1). Oligo(dT) magnetic beads were used to obtain the purified mRNA, which was divided into smaller fragments. First-strand cDNA was generated by random hexamer-primed reverse transcription, followed by second-strand cDNA synthesis. The synthesized cDNA was subjected to end-repair and 3' adenylation and the adapters were ligated to the ends of the 3' adenylated cDNA fragments. The cDNA was amplified by PCR and the products were purified using Ampure XP beads (Agencourt; Beckman Coulter, Inc.) and dissolved in ethidium bromide solution. The double-stranded PCR products were denatured and circularized according to the splint oligo sequence to obtain the final library. Single-stranded circular DNA was designated as the final library. For quality control (QC), the library was validated using the Agilent Technologies 2100 bioanalyzer (Agilent Technologies, Inc.). The Standard Sensitivity RNA Analysis Kit (15 nt, DNF-471; Agilent Technologies, Inc.) was used as a detection kit for this section.

Transcriptome sequencing. The final library was amplified with ϕ29 DNA polymerase to make DNA nanoballs (DNBs), which had more than 300 copies of each molecule. The DNBs were loaded onto the patterned nanoarray and 150 paired-end base reads were generated using combinatorial probe-anchor synthesis on the BGIseq500 platform (BGI Group).

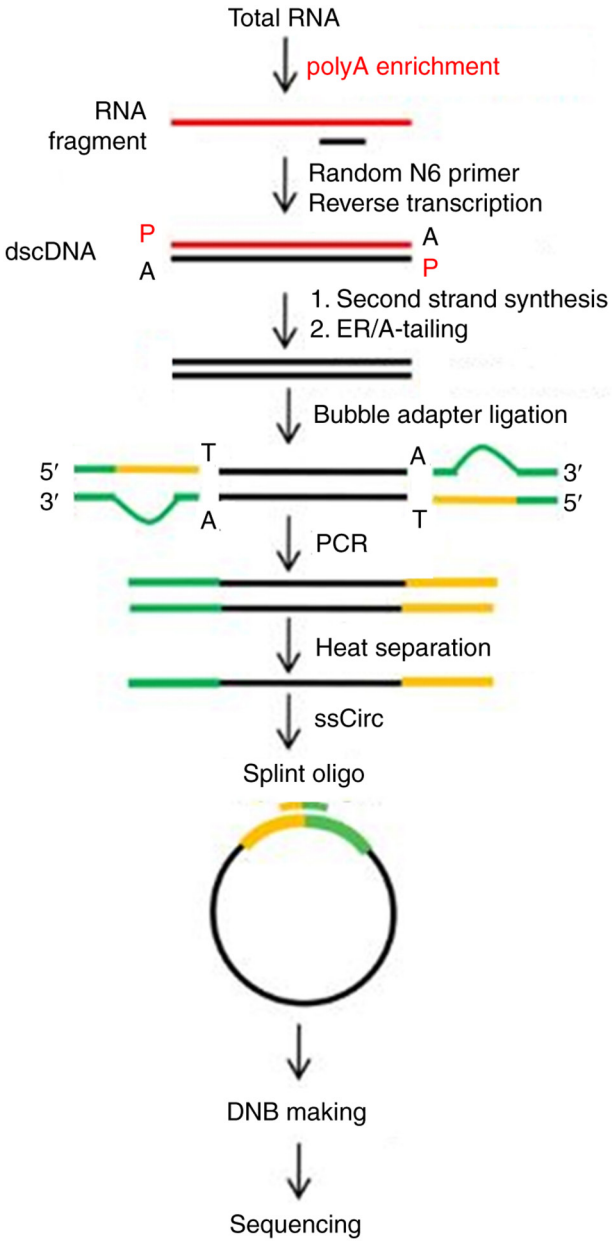

Figure 1. mRNA library construction and transcriptome sequencing. DNB, DNA nanoball.

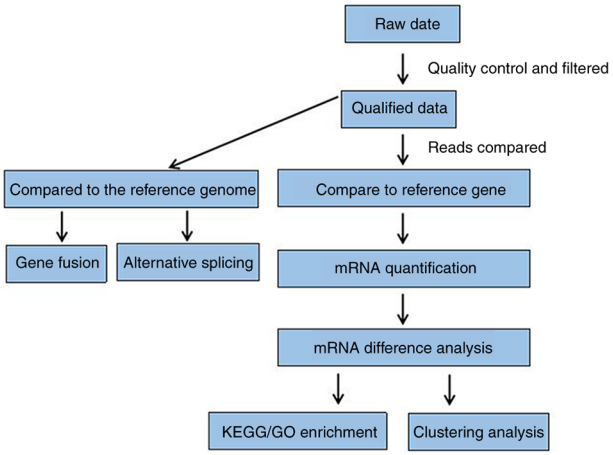

Figure 2. Flow chart of bioinformatics analysis. KEGG, Kyoto Encyclopedia of Genes and Genomes; GO, Gene Ontology.

Bioinformatics analysis. The mouse (Mus_musculus; GCF_000001635.26_GRCm38.p6; NCBI) genome served as the reference genome. The sequencing reads were compared against the reference genome to annotate and quantify the genes.

The sequencing data were designated as raw reads or raw data. QC was performed on the raw reads and the qualified data was used for subsequent analyses. After QC, the filtered clean reads were compared to the reference sequences. Using the statistical comparison rate and the distribution of reads of the reference sequences, we determined whether the comparison results passed the second QC (QC of alignment). After the QC was qualified, the quantitative analysis of genes and the analysis of gene expression levels (principal components, correlation scores, differential gene screening) were performed. Additional analyses were carried out for selected differentially expressed genes (DEGs) such as Gene Ontology (GO; http://geneontology.org/) term enrichment analysis, Kyoto Encyclopedia of Genes and Genomes (KEGG; https://www.genome.jp/kegg/) pathway enrichment analysis, gene expression clustering analysis, SNP (single nucleotide polymorphism) and InDell analyses and splicing gene event analysis (Fig. 2).

The sequencing data were filtered using SOAPnuke software (v1.5.2, https://github.com/BGI-flexlab/SOAPnuke) as follows: i) Reads containing a junction (junction contamination) were removed; ii) reads containing >5% of unknown bases were eliminated; and iii) low quality reads (reads with a mass value <10, accounting for >20% of the total bases as low quality reads) were removed. The filtered 'clean reads' were saved in FASTQ format.

Sample correlation analysis. Pearson correlation coefficients for all gene expression levels between the two samples were calculated and presented as heat maps to reflect the correlations between the gene expression levels (the higher the correlation coefficient, the more similar the gene expression level).

Gene expression distribution analysis. The distribution of gene expression levels was presented as box plots and the dispersion of the distributed data was observed. The trends in the gene abundance and the expression level were presented as density maps and the intervals of the gene expression concentration areas were also analyzed. At the same time, the gene number of the expected number of fragments per kilobase of transcript sequence per million base pairs sequenced (FPKM; FPKM ≤1, FPKM=1-10, FPKM ≥10) in the three cases was counted using stacked bar graphs, so as to visually display the gene numbers in different FPKM intervals for each sample.

Differential expression analysis. Differential expression analysis of the paired groups was performed using the DESeq 2 method (22). The screening conditions were as follows: the difference multiple |log2FC| ≥1 and Q value ≤0.05. Volcano maps were generated and analyzed to identify the upregulated and downregulated DEGs.

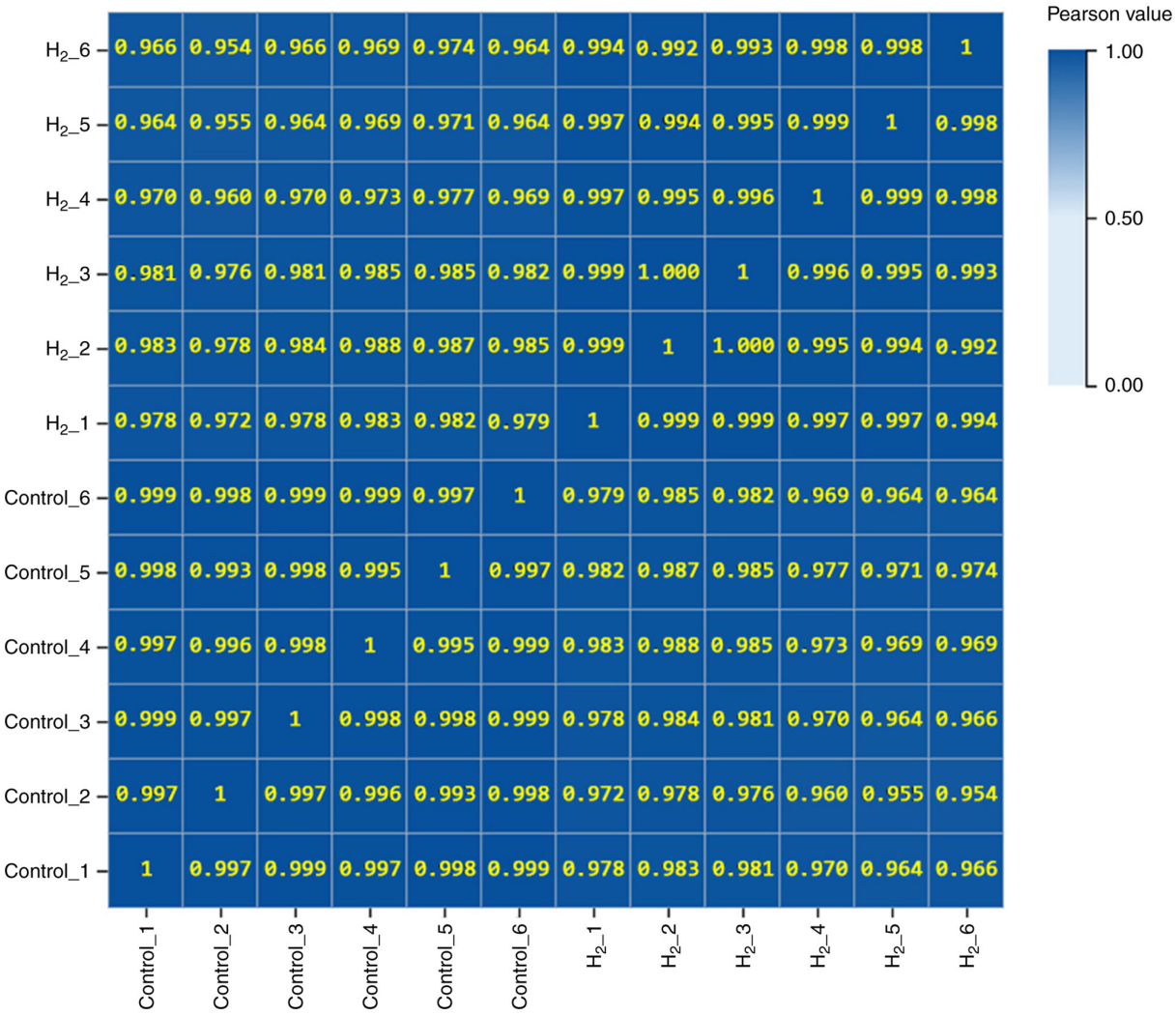

Figure 3. Sample correlation thermogram. The x- and y-axes represent samples and the color represents the correlation coefficient (the darker the color, the higher the correlation; the lighter the color, the lower the correlation).

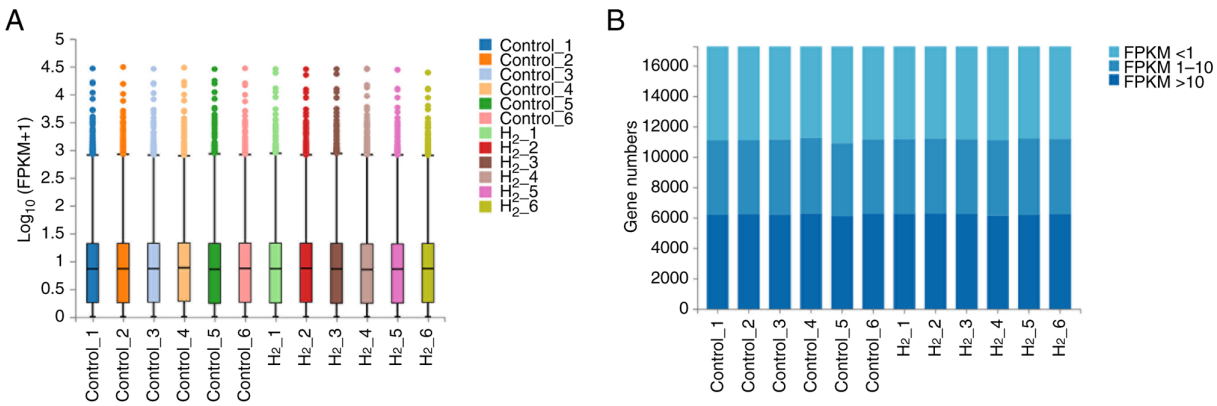

Figure 4. Box plot diagram of the gene expression level and stacked histogram of the gene number accumulation in different FPKM intervals. In the box plot diagram (A), each box plot corresponds to five statistics, namely, upper limit, upper quartile, median, lower quartile and lower limit. In the stacked histogram (B), the color corresponds to different expression levels: genes with FPKM <1 had extremely low expression, genes with FPKM between 1 and 10 had low expression levels and genes with FPKM >10 had medium and high expression levels. FPKM, expected number of fragments per kilobase of transcript sequence per millions base pairs sequenced.

Differential cluster analysis. According to the results of the identified DEGs, the R project pheatmap tool (v1.0.12, https://cran.r-project.org/web/packages/pheatmap/) was used for hierarchical clustering analysis. In terms of the gene expression, Bowtie 2 software (v2.2.5, http://bowtie-bio.sourceforge.net/bowtie2/index.shtml) (23) was used to compare the clean

Table I. Gene number distribution of both groups in different FPKM intervals.

FPKM intervals	≥10	~1-10	≤1
H_2 group	6,234.3±51.52	4,945.3±30.98	6,087.0±41.17
Control group	6,215.0±66.37	4,900.5±53.39	6,151.5±111.92

FPKM, expected number of fragments per kilobase of transcript sequence per millions base pairs sequenced.

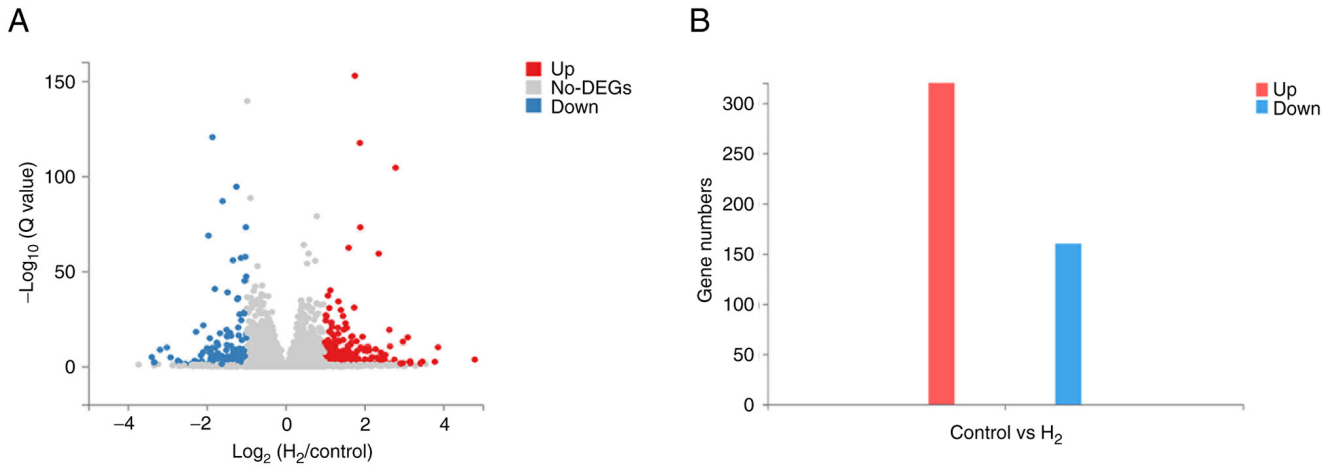

Figure 5. (A) Volcano map and (B) statistical map of DEGs. The upregulated DEGs are represented in red, the downregulated DEGs are represented in blue and the non-DEGs are represented in gray. DEG, differentially expressed gene.

reads to the reference gene sequences and RSEM software (v1.2.8, http://deweylab.biostat.wisc.edu/rsem/rsem-calculate-expression.html) was used to calculate the gene expression level of each sample (24).

GO term enrichment analysis and GO annotation classification of DEGs. Enrichment analysis was used to determine whether each DEG was significantly enriched in terms of a specific molecular function, biological process, or metabolic pathway. According to the results of the GO annotations, the DEGs were classified according to their function. The phyper function within R software (v4.1.0, https://stat.ethz.ch/R-manual/R-devel/library/stats/html/Hypergeometric.html) was used for enrichment analysis and P-values were calculated. The false discovery rate (FDR) correction was performed using the P-value (v2.26.0, https://bioconductor.org/packages/release/bioc/html/qvalue.html) to obtain the *Q*-value. The GO terms that satisfied the *Q*-value ≤0.05 criterion were defined as significantly enriched and DEGs were assigned different biological functions. According to the results of the GO annotations, the DEGs were divided into three functional categories; molecular functions, cellular components and biological processes.

KEGG pathway enrichment analysis and KEGG annotation classification of DEGs. According to the results of the KEGG pathway annotations, the phyper function within R software was used for enrichment analysis. The FDR correction was performed using the P-value to obtain the *Q*-value. The unigenes that satisfied the *Q*-value ≤0.05 criterion were significantly expressed in GO term and KEGG pathway analyses. KEGG metabolic pathways related to DEGs were divided into seven categories: Cellular processes, environmental information processing, genetic information processing, human diseases (animal only), metabolic processes, organic systems and drug development. Pathway enrichment analysis determined the main biochemical metabolic pathways and signal transduction pathways related to the DEGs.

Alternative splicing and differential alternative splicing analysis. Following filtering, the clean reads were compared with the reference genome for reference genome alignment using HISAT 2 software (v2.0.4, http://www.ccb.jhu.edu/software/hisat) (25). The alternative splicing events and the differential alternative splicing events between the two groups were identified by rMATS software (v3.2.5, http://rnaseq-mats.sourceforge.net) (26). The alternative splicing events were skipped exons (SE), alternative 5' splicing sites, alternative 3' splicing sites (A3SS), mutually exclusive exons and retained introns (RI).

Gene fusion analysis. Gene fusion is the process by which a portion or the whole sequence of one gene is fused with that of another gene to form a new gene. Ericscript software (v0.5.5, http://ericscript.sourceforge.net/) (27) was used for gene fusion analysis and gene fusion events were identified by comparing the sequences of paired-end relationships between the genome and the transcript. The mechanisms of gene fusion were chromosome translocations, intermediate deletions, chromosome inversions and trans splicing.

Target gene analysis. According to the expression and the enrichment of the DEGs, the target genes and related signaling pathways involved in the H_2-mediated inhibition of BMMC osteoclastogenesis were predicted and analyzed.

Statistical analysis. Continuous variables were presented as the mean ± standard deviation ($X \pm S$). The results were analyzed by one-way ANOVA, followed by LSD or Dunnett's multiple comparison test, or by Student's *t*-test using SPSS 19.0 software (IBM Corp.). P<0.05 was considered to indicate a statistically significant difference.

Results

In the present study, 12 samples were sequenced and analyzed using the BGISEQ-500 platform. On average, each sample yielded 6.71G of data and a total of 17,267 genes were detected. For the clean reads of the H_2 group and the control group, the average comparison rates to the reference genome were 92.54 and 93.29%, respectively; and the average comparison rates to the reference gene set were 75.75 and 76.84%, respectively. All the rates were >70.00%, indicating that the reference genome selection was appropriate. According to the clean reads sequencing data of the H_2 group and the control group, the 99.00% base correct recognition rates (Q20) were 96.05 and 96.49%, respectively and the 99.90% base correct recognition rates (Q30) were 86.78 and 87.79%, respectively. The sequencing quality met the requirements of subsequent analysis.

Samples show good biological repetition. As shown in Fig. 3, Pearson correlation coefficient analysis revealed that the correlation coefficient between any two samples was >0.95, indicating that the gene expression levels among the samples were very similar and the samples showed good biological repetition.

Gene expression distribution analysis shows that the sequencing data are well standardized. The sequencing data were standardized and a box plot distribution of the gene expression levels of each sample is shown in Fig. 4A. The median of the box plot of each sample was aligned. The stacked histogram results of the gene number accumulation in different FPKM intervals of the H_2 group and the control group were shown in Fig. 4B and Table I. The differences in the gene number of the medium-high expression level (t=-0.564; P=0.585), low expression level (t=-1.779; P=0.106), or very low expression level (t=1.318; P=0.217) were not statistically significant. The gene expression box plot and the gene number stacked histogram showed that the sequencing data were well standardized and met the experimental requirements.

DEGs identified and their expression levels. In this experiment, the criteria for identifying the DEGs were as follows: |log2FC| ≥1 and *Q*-value ≤0.05. The results showed that there were 480 DEGs between the H_2 group and the control group. Among them, 320 DEGs were upregulated and 160 DEGs were downregulated (Fig. 5).

As shown in Fig. 6, the results of RNA-seq cluster analysis showed that the H_2 group and the control group could be completely separated and the corresponding gene expression patterns of the two groups were significantly different. The high expression values of the DEGs in the grouped samples are represented in red and the low expression values of the DEGs in the grouped samples are represented in blue.

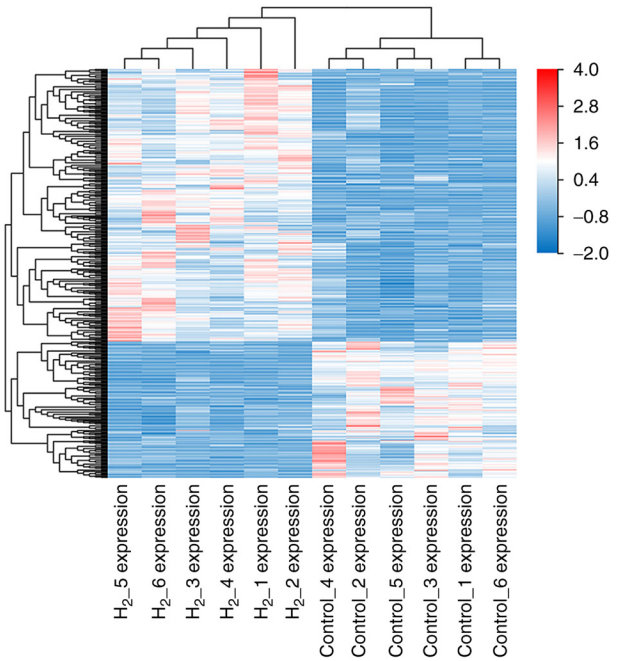

Figure 6. Cluster heat map of DEGs. The horizontal axis was $\log_2$ (expression value + 1) and the vertical axis was the gene. The redder the color, the higher the gene expression; the bluer the color, the lower the gene expression. DEG, differentially expressed gene.

GO term enrichment and KEGG pathway enrichment of DEGs. As shown in Table II, among the GO enriched terms, the top five enriched gene terms for cellular components were mainly related to extracellular region, extracellular space, extracellular matrix, collagen-containing extracellular matrix and collagen trimer. The top five enriched gene terms for molecular functions were mainly related to extracellular matrix structural constituent, growth factor activity, heparin binding, extracellular matrix structural constituent conferring tensile strength and aldehyde dehydrogenase activity. The top five enriched gene terms for biological processes were mainly related to regulation of signaling receptor activity, immune response, positive regulation of angiogenesis, cholesterol biosynthesis and sterol biosynthesis.

As shown in Table III, among the KEGG pathway enriched terms, the top five enriched pathway terms were mainly related to ECM-receptor interactions, protein digestion and absorption, TNF signaling pathway, terpenoid backbone biosynthesis and sesquiterpenoid and triterpenoid biosynthesis.

Main types of gene variations. The results showed that the main alternative splicing events between the H_2 group and the control group were RI and SE, which accounted for 39.04 and 32.62% of splicing events, respectively (Fig. 7 and Table IV).

As shown in Table V, the analysis of gene fusion events in the H_2 group and the control group showed that different degrees of gene fusion occurred in both groups. The most

Table II. GO enrichment analysis of differentially expressed genes.

Term type	Term ID	Term description	Term candidate gene num	Rich ratio	*Q*-value
GO_C	GO:0005576	Extracellular region	99	0.052519894	$1.41x10^{-15}$
	GO:0005615	Extracellular space	87	0.050464037	$1.25x10^{-12}$
	GO:0031012	Extracellular matrix	30	0.107142857	$2.78x10^{-11}$
	GO:0062023	Collagen-containing extracellular matrix	27	0.088815789	$2.56x10^{-8}$
	GO:0005581	Collagen trimer	13	0.141304348	$4.34x10^{-6}$
GO_F	GO:0005201	Extracellular matrix structural constituent	16	0.130081301	$5.22x10^{-6}$
	GO:0008083	Growth factor activity	16	0.101910828	$6.58x10^{-5}$
	GO:0008201	Heparin binding	17	0.094972067	$6.58x10^{-5}$
	GO:0030020	Extracellular matrix structural constituent conferring tensile strength	8	0.205128205	$2.24x10^{-4}$
	GO:0004030	Aldehyde dehydrogenase [NAD(P)+] activity	3	0.75	$3.26x10^{-3}$
GO_P	GO:0010469	Regulation of signaling receptor activity	35	0.079726651	$3.22x10^{-8}$
	GO:0006955	Immune response	26	0.083601286	$1.80x10^{-6}$
	GO:0045766	Positive regulation of angiogenesis	18	0.120805369	$1.80x10^{-6}$
	GO:0006695	Cholesterol biosynthetic process	9	0.264705882	$1.35x10^{-5}$
	GO:0016126	Sterol biosynthetic process	8	0.275862069	$4.35x10^{-5}$

GO, Gene Ontology.

Table III. KEGG pathway enrichment analysis of differentially expressed genes.

Term ID	Term description	Term candidate gene number	Rich ratio	Q-value
04512	ECM-receptor interaction	12	0.130434783	$3.22x10^{-4}$
04974	Protein digestion and absorption	12	0.12244898	$3.22x10^{-4}$
04668	TNF signaling pathway	13	0.092198582	$1.94x10^{-3}$
00900	Terpenoid backbone biosynthesis	5	0.185185185	$1.80x10^{-2}$
00909	Sesquiterpenoid and triterpenoid biosynthesis	2	1	$1.96x10^{-2}$

KEGG, Kyoto Encyclopedia of Genes and Genomes.

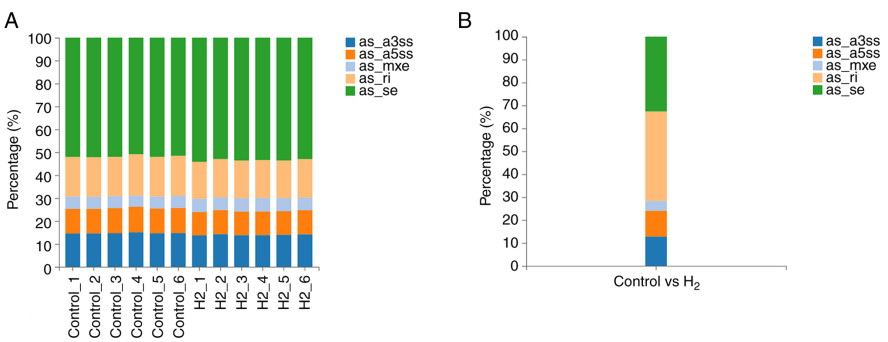

Figure 7. Alternative splicing event and differential alternative splicing event. The x-axis represents the sample (or comparison group) and the y-axis represents the proportion of different alternative splicing types in the corresponding sample (or comparison group). Each color corresponds to a type of alternative splicing. (A) Alternative splicing event. (B) Differential alternative splicing event.

common type of gene fusion event was inter-chromosomal, in addition to a small number of intra-chromosomal and read-through events.

Target genes and possible signaling pathways. The analysis of the expression of DEGs, as well as GO terms and KEGG pathways, identified a variety of targets involved in the

Table IV. Different alternative splicing events between groups.

Type	SE	A5SS	A3SS	MXE	RI
Percentage	32.62%	11.23%	12.83%	4.28%	39.04%
Number	61	21	24	8	73

SE, skipped exons; A5SS, alternative 5' splicing sites; A3SS, alternative 3' splicing sites; MXE, mutually exclusive exons; RI, retained introns.

Table V. Gene fusion events.

Sample	Upstream fusion gene	Downstream fusion gene	Types
H_2_1	14593, NC_000079.6	235184, NC_000075.6	Inter-chromosomal
	18733, NC_000073.6	100038909, NC_000073.6	Intra-chromosomal
H_2_2	104662, NC_000077.6	27364, NC_000077.6	Read-Through
	20363, NC_000081.6	13030, NC_000080.6	Inter-chromosomal
H_2_3	66713, NC_000077.6	11816, NC_000073.6	Inter-chromosomal
	75826, NC_000082.6	228880, NC_000068.7	Inter-chromosomal
	14127, NC_000067.6	242341, NC_000070.6	Inter-chromosomal
H_2_4	215449, NC_000076.6	268566, NC_000078.6	Inter-chromosomal
	18787, NC_000071.6	12846, NC_000082.6	Inter-chromosomal
H_2_5	72543, NC_000068.7	13135, NC_000080.6	Inter-chromosomal
	19025, NC_000068.7	19156, NC_000076.6	Inter-chromosomal
H_2_6	None	None	None
Control_1	None	None	None
Control_2	238564, NC_000079.6	21354, NC_000083.6	Inter-chromosomal
	233895, NC_000073.6	15042, NC_000083.6	Inter-chromosomal
	70750, NC_000067.6	114893, NC_000069.6	Inter-chromosomal
	50911, NC_000069.6	12428, NC_000069.6	Read-Through
Control_3	67707, NC_000069.6	55982, NC_000071.6	Inter-chromosomal
Control_4	14127, NC_000067.6	20583, NC_000082.6	Inter-chromosomal
	100042025, NC_000087.7	19156, NC_000076.6	Inter-chromosomal
Control_5	None	None	None
Control_6	17876, NC_000068.7	67179, NC_000080.6	Inter-chromosomal
	12986, NC_000070.6	223658, NC_000081.6	Inter-chromosomal
	66129, NC_000079.6	21804, NC_000073.6	Inter-chromosomal

H_2-mediated inhibition of BMMC osteoclastogenesis as follows: *Fos*, *Dusp1*, *Cxcl1*, *Reln*, *Itga2b*, *Plin2*, *Lif*, *Thbs1*, *Vegfa* and *Gadd45a* (all upregulated) and *Hspa1b*, *Gm4951*, *F830016B08Rik*, *Fads2*, *Hspa1a*, *Slc27a6*, *Cacna1b*, *Scd2*, *Lama3* and *Col4a5* (all downregulated). The analysis also identified a variety of signaling pathways involved in immunity, inflammation, oxidative stress and apoptosis as follows: osteoclast differentiation cascades, as well as PI3K-AKT, FoxO, MAPK, PPAR, TNF, TGF-β, JAK-STAT, RAS, VEGF, HIF-1 and AMPK signaling pathways (Table VI).

Discussion

RNA-sequencing (quantification) is based on next-generation high-throughput sequencing technologies that provide accurate digital expression profiling information by measuring transcript sequence levels and performing comparative analyses to study the expression pattern of eukaryotic genes. Transcriptome research is the basis and the starting point of gene function and structure research, through which researchers can comprehensively and quickly obtain almost all the transcript sequence information for a specific tissue or organ of a certain species under specific conditions.

In the present study, RNA-seq was used to study the transcriptome of mouse BMMCs exposed to H_2 in an osteoclast-induced environment. The main signaling pathways of DEGs were identified and they were involved in immunity, inflammation, apoptosis and cell differentiation. Our previous study reported that H_2 could inhibit BMMC osteoclastogenesis in mice (18). H_2 can penetrate membranes and enter cells, where it behaves as an antioxidant, inhibiting the differentiation of BMMCs to osteoclasts (28-30). It is well known that reactive oxygen species (ROS) (31), such as hydrogen peroxide (32) and superoxide dismutase (33), are osteoclast inducing factors, but

Table VI. Differentially expressed genes and signaling pathways.

Type	Gene ID	Gene symbol	$\log_2$ (H_2/Control)	*Q*-value	KEGG pathway
Up	14281	Fos	1.882	$3.41x10^{-118}$	MAPK signaling pathway
					TNF signaling pathway
	19252	Dusp1	1.756	$1.72x10^{-153}$	MAPK signaling pathway
	14825	Cxcl1	1.474	$4.02x10^{-20}$	TNF signaling pathway
	19699	Reln	1.388	$3.41x10^{-8}$	PI3K-Akt
	16399	Itga2b	1.359	$7.16x10^{-14}$	PI3K-Akt signaling pathway
	11520	Plin2	1.340	$6.69x10^{-35}$	PPAR signaling pathway
	16878	Lif	1.332	$5.84x10^{-18}$	Jak-STAT signaling pathway
					TNF signaling pathway
	21825	Thbs1	1.217	$5.06x10^{-17}$	PI3K-Akt signaling pathway
					TGF-β signaling pathway
	22339	Vegfa	1.111	$4.04x10^{-19}$	Ras signaling pathway
					MAPK signaling pathway
					VEGF signaling pathway
					HIF-1 signaling pathway
					PI3K-Akt signaling pathway
	13197	Gadd45a	1.034	$3.56x10^{-27}$	FoxO signaling pathway
					MAPK signaling pathway
					p53 signaling pathway
Down	15511	Hspa1b	-1.201	$3.10x10^{-21}$	MAPK signaling pathway
	240327	Gm4951	-1.222	$3.78x10^{-36}$	TNF signaling pathway
	240328	F830016B08Rik	-1.334	$1.61x10^{-56}$	TNF signaling pathway
	56473	Fads2	-1.381	$7.36x10^{-17}$	PPAR signaling pathway
	193740	Hspa1a	-1.478	$1.76x10^{-16}$	MAPK signaling pathway
	225579	Slc27a6	-1.500	$2.42x10^{-9}$	PPAR signaling pathway
	12287	Cacna1b	-1.710	$6.22x10^{-12}$	MAPK signaling pathway
	20250	Scd2	-1.793	$1.67x10^{-41}$	AMPK signaling pathway
					PPAR signaling pathway
	16774	Lama3	-1.793	$2.24x10^{-6}$	PI3K-Akt signaling pathway
	12830	Col4a5	-1.905	$1.56x10^{-8}$	PI3K-Akt signaling pathway

PPAR, peroxisome proliferator-activated receptor; HIF-1, hypoxia-inducible factor; FoxO, forkhead box O.

they are reversely regulated by H_2, possibly due to its strong reducing agent effect. Although several studies have reported that ROS regulate osteoclastogenesis (34-37), the existing studies have not reported the possible signaling pathways that are involved in this process.

Fan *et al* (38) demonstrated that H_2-rich saline could decrease the expression levels of IL-6, JAK, STAT-3 and other signaling proteins by inhibiting the JAK-STAT signaling pathway, thereby inhibiting myocardial hypertrophy in rats. Chen *et al* (39) reported that H_2 exerts anti-apoptotic effects by inhibiting Ras-ERK1/2-MEK1/2 and AKT signaling pathways in rat vascular smooth muscle cells. At the same time, other studies have shown that H_2 could alleviate the damage induced by lipopolysaccharides in an acute lung injury model (40); H_2 can also upregulate the expression of claudin-5 by activating the PI3K/AKT signaling pathway in alveolar epithelial cells, thereby reducing cell permeability and improving pulmonary edema (41). Other studies have demonstrated that H_2 can exert antioxidant, anti-inflammatory and anti-apoptotic effects by inhibiting p38-MAPK (42), JNK-caspase 3 (40) and NF-kB (11,43) signaling pathways, in addition to NRF2, WNT/β-catenin, thioredoxin interaction protein/NLR3 inflammasome and RHO/ROCK signaling pathways.

The results of the above studies using different cell or animal models were basically consistent with the results of the present study. However, based on the results of gene enrichment analysis, the present study identified new signaling pathways that may have roles in BMMC osteoclastogenesis, including FoxO, PPAR, TNF, TGF-β, VEGF, HIF-1 and AMPK signaling pathways. These signaling pathways have roles in immunity, inflammation, proliferation, differentiation, apoptosis, cell cycle regulation and metabolism. At the same time, the findings of the present study were different from those of previous studies. For example, the studies of Takayanagi *et al* (44), Grigoriadis *et al* (45) and Jiao *et al* (46) showed that the *Fos* gene was an osteoclast-inducible gene,

but the present study showed that H_2 inhibited osteoclast differentiation and the *Fos* gene was highly expressed. The reason for this difference may be due to the different cells and culture methods used in the different experiments, or it may be due to other reasons that are currently unknown. Therefore, further studies are needed to determine whether these genes have biological effects on BMMCs through specific signaling pathways in an osteoclast-induced environment and the results should be compared with those of previous studies.

It is well known that osteoclasts serve an important role in the occurrence and development of osteoporosis and the present study showed that H_2 could inhibit the differentiation of osteoclasts by acting on related genes through certain signaling pathways. This may be the mechanism by which H_2 exerts its anti-osteoporosis effects. H_2 is generated during the degradation of Mg alloys and the formation of osteoclasts can be inhibited by H_2, so Mg alloys indirectly exert their anti-osteoporosis effects. Our previous study revealed that H_2 can inhibit BMMC osteoclastogenesis in mice (18). However, the mechanism by which this occurs, which is critical for the translational research of H_2 and Mg alloys and the treatment of osteoporosis, is still unclear. The present study used transcriptome sequencing to identify the possible mechanism behind the H_2-mediated inhibition of osteoclastogenesis and revealed the key genes and signaling pathways involved, thereby providing a theoretical basis for the significance of H_2 and an experimental basis for the application of Mg alloys in the treatment of fractures, bone defects and osteoporosis.

There were several limitations to the present study. First, although the primary mouse BMMCs used in this study were isolated as previously described (20,21), the cell populations were not well identified. Second, the possible molecular mechanism by which H_2 inhibits BMMC osteoclastogenesis was not thoroughly studied. Thus, further studies are needed to determine whether H_2 inhibits BMMC osteoclastogenesis through these pathways.

The present study is the first to investigate the transcriptome of mouse BMMCs exposed to H_2 in an osteoclast-induced environment by RNA-seq, to the best of the authors' knowledge. The results showed that there were 480 DEGs between the H_2 group and the control group. Among them, 320 DEGs were upregulated (*Fos*, *Dusp1*, *Cxcl1*, *Reln*, *Itga2b*, *Plin2*, *Lif*, *Thbs1*, *Vegfa* and *Gadd45a*) and 160 DEGs were downregulated (*Hspa1b*, *Gm4951*, *F830016B08Rik*, *Fads2*, *Hspa1a*, *Slc27a6*, *Cacna1b*, *Scd2*, *Lama3* and *Col4a5*). Comprehensive analysis of DEGs, as well as GO terms and KEGG pathways, revealed that these DEGs were mainly involved in osteoclast differentiation cascades, as well as PI3K-AKT, FoxO, MAPK, PPAR, TNF, TGF-β, JAK-STAT, RAS, VEGF, HIF-1 and AMPK signaling pathways, which are involved in immunity, inflammation, apoptosis and cell differentiation. At the same time, the main alternative splicing events between the H_2 group and the control group were RI and SE. Gene fusion occurred in both groups and inter-chromosomal fusion was the main way by which genes were fused. Therefore, the results of the present study revealed the possible target genes and signaling pathways of H_2-mediated BMMC osteoclastogenesis and provided a theoretical basis for exploring the feasibility of H_2 in the treatment of osteoporosis.

Acknowledgements

Not applicable.

Funding

The present study was supported by the State Key Laboratory of Metal Matrix Composites, Shanghai Jiao Tong University (grant no. mmc-kf20-02) and the San-Ming Project of Medicine in Shenzhen (grant no. SZSM201612092).

Availability of data and materials

The datasets generated and/or analyzed during the current study are available in the NCBI repository, https://www.ncbi.nlm.nih.gov/sra/PRJNA865067.

Authors' contributions

YL, WW, YZ and HZ developed the concepts in this study. YL performed the experiments, collected and analyzed the data and wrote the manuscript. YL and WW confirm the authenticity of all the raw data. All authors read and approved the final manuscript.

Ethics approval and consent to participate

The present study was conducted in accordance with the ethical standards of the Ethics Committee of Peking University Shenzhen Hospital, who approved the experimental protocols.

Patient consent for publication

Not applicable.

Competing interests

The authors declare that they have no competing interests.

References

1. Agarwal S, Curtin J, Duffy B and Jaiswal S: Biodegradable magnesium alloys for orthopaedic applications: A review on corrosion, biocompatibility and surface modifications. Mater Sci Eng C Mater Biol Appl 68: 948-963, 2016.
2. Maradze D, Musson D, Zheng Y, Cornish J, Lewis M and Liu Y: High magnesium corrosion rate has an effect on osteoclast and mesenchymal stem cell role during bone remodelling. Sci Rep 8: 10003, 2018.
3. Zhang Y, Xu J, Ruan YC, Yu MK, O'Laughlin M, Wise H, Chen D, Tian L, Shi D, Wang J, *et al*: Implant-derived magnesium induces local neuronal production of CGRP to improve bone-fracture healing in rats. Nat Med 22: 1160-1169, 2016.
4. Zhai Z, Qu X, Li H, Yang K, Wan P, Tan L, Ouyang Z, Liu X, Tian B, Xiao F, *et al*: The effect of metallic magnesium degradation products on osteoclast-induced osteolysis and attenuation of NF-κB and NFATc1 signaling. Biomaterials 35, 6299-6310, 2014.
5. Luo Y, Wang J, Ong MTY, Yung PS, Wang J and Qin L: Update on the research and development of magnesium-based biodegradable implants and their clinical translation in orthopaedics. Biomater Transl 2: 188-196, 2021.
6. Lin Y, Ohkawara B, Ito M, Misawa N, Miyamoto K, Takegami Y, Masuda A, Toyokuni S and Ohno K: Molecular hydrogen suppresses activated Wnt/β-catenin signaling. Sci Rep 6: 31986, 2016.

7. Guo JD, Li L, Shi YM, Wang HD and Hou SX: Hydrogen water consumption prevents osteopenia in ovariectomized rats. Br J Pharmacol 168: 1412-1420, 2013.
8. Sun Y, Shuang F, Chen DM and Zhou RB: Treatment of hydrogen molecule abates oxidative stress and alleviates bone loss induced by modeled microgravity in rats. Osteoporos Int 24: 969-978, 2013.
9. Yoneda T, Tomofuji T, Kunitomo M, Ekuni D, Irie K, Azuma T, Machida T, Miyai H, Fujimori K and Morita M: Preventive effects of drinking hydrogen-rich water on gingival oxidative stress and alveolar bone resorption in rats fed a high-fat diet. Nutrients 9: 64, 2017.
10. Callaway DA and Jiang JX: Reactive oxygen species and oxidative stress in osteoclastogenesis, skeletal aging and bone diseases. J Bone Miner Metab 33: 359-370, 2015.
11. Li DZ, Zhang QX, Dong XX, Li HD and Ma X: Treatment with hydrogen molecules prevents RANKL-induced osteoclast differentiation associated with inhibition of ROS formation and inactivation of MAPK, AKT and NF-κB pathways in murine RAW264.7 cells. J Bone Miner Metab 32: 494-504, 2014.
12. Boyde A, Ali NN and Jones SJ: Resorption of dentine by isolated osteoclasts in vitro. Br Dent J 156: 216-220, 1984.
13. Chambers TJ, Revell PA, Fuller K and Athanasou NA: Resorption of bone by isolated rabbit osteoclasts. J Cell Sci 66: 383-399, 1984.
14. Destaing O, Saltel F, Géminard JC, Jurdic P and Bard F: Podosomes display actin turnover and dynamic self-organization in osteoclasts expressing actin-green fluorescent protein. Mol Biol Cell 14: 407-416, 2003.
15. Parfitt AM: Targeted and nontargeted bone remodeling: Relationship to basic multicellular unit origination and progression. Bone 30: 5-7, 2002.
16. Manolagas SC: Birth and death of bone cells: Basic regulatory mechanisms and implications for the pathogenesis and treatment of osteoporosis. Endocr Rev 21: 115-137, 2000.
17. Toor SM, Wani S and Albagha OME: Comprehensive transcriptomic profiling of murine osteoclast differentiation reveals novel differentially expressed genes and LncRNAs. Front Genet 12: 781272, 2021.
18. Liu Y, Wang DL, Huang YC, Wang TB and Zeng H: Hydrogen inhibits the osteoclastogenesis of mouse bone marrow mononuclear cells. Mater Sci Eng C Mater Biol Appl 110: 110640, 2020.
19. Chen X, Cui J, Zhai X, Zhang J, Gu Z, Zhi X, Weng W, Pan P, Cao L, Ji F, *et al*: Inhalation of hydrogen of different concentrations ameliorates spinal cord injury in mice by protecting spinal cord neurons from apoptosis, oxidative injury and mitochondrial structure damages. Cell Physiol Biochem 47: 176-190, 2018.
20. Zhang Y, Guan H, Li J, Fang Z, Chen W and Li F: Amlexanox suppresses osteoclastogenesis and prevents Ovariectomy-Induced bone loss. Sci Rep 5: 13575, 2015.
21. Chen X, Zhi X, Cao L, Weng W, Pan P, Hu H, Liu C, Zhao Q, Zhou Q, Cui J and Su J: Matrine derivate MASM uncovers a novel function for ribosomal protein S5 in osteoclastogenesis and postmenopausal osteoporosis. Cell Death Dis 8: e3037, 2017.
22. Love MI, Huber W and Anders S: Moderated estimation of fold change and dispersion for RNA-seq data with DESeq2. Genome Biol 15: 550, 2014.
23. Langmead B and Salzberg SL: Fast gapped-read alignment with Bowtie 2. Nat Methods 9: 357-359, 2012.
24. Li B and Dewey CN: RSEM: Accurate transcript quantification from RNA-Seq data with or without a reference genome. BMC Bioinformatics 12: 323, 2011.
25. Kim D, Langmead B and Salzberg SL: HISAT: A fast spliced aligner with low memory requirements. Nat Methods 12: 357-360, 2015.
26. Shen S, Park JW, Lu ZX, Lin L, Henry MD, Wu YN, Zhou Q and Xing Y: rMATS: Robust and flexible detection of differential alternative splicing from replicate RNA-Seq data. Proc Natl Acad Sci USA 111: 5593-5601, 2014.
27. Benelli M, Pescucci C, Marseglia G, Severgnini M, Torricelli F and Magi A: Discovering chimeric transcripts in paired-end RNA-seq data by using EricScript. Bioinformatics 28: 3232-3239, 2012.
28. Guo J, Dong W, Jin L, Wang P, Hou Z and Zhang Y: Hydrogen-rich saline prevents bone loss in diabetic rats induced by streptozotocin. Int Orthop 41: 2119-2128, 2017.
29. Ohsawa I, Ishikawa M, Takahashi K, Watanabe M, Nishimaki K, Yamagata K, Katsura K, Katayama Y, Asoh S and Ohta S: Hydrogen acts as a therapeutic antioxidant by selectively reducing cytotoxic oxygen radicals. Nat Med 13: 688-694, 2007.
30. Wu D, Liang M, Dang H, Fang F, Xu F and Liu C: Hydrogen protects against hyperoxia-induced apoptosis in type II alveolar epithelial cells via activation of PI3K/Akt/Foxo3a signaling pathway. Biochem Biophys Res Commun 495, 1620-1627, 2018.
31. Chen K, Liu Y, He J, Pavlos N, Wang C, Kenny J, Yuan J, Zhang Q, Xu J and He W: Steroid-induced osteonecrosis of the femoral head reveals enhanced reactive oxygen species and hyperactive osteoclasts. Int J Biol Sci 16: 1888-1900, 2020.
32. Bartell SM, Kim HN, Ambrogini E, Han L, Iyer S, Serra Ucer S, Rabinovitch P, Jilka RL, Weinstein RS, Zhao H, *et al*: FoxO proteins restrain osteoclastogenesis and bone resorption by attenuating H_2O_2 accumulation. Nat Commun 5: 3773, 2014.
33. Kim H, Lee YD, Kim HJ, Lee ZH and Kim HH: SOD2 and Sirt3 control osteoclastogenesis by regulating mitochondrial ROS. J Bone Miner Res 32: 397-406, 2017.
34. Lee NK, Choi YG, Baik JY, Han SY, Jeong DW, Bae YS, Kim N and Lee SY: A crucial role for reactive oxygen species in RANKL-induced osteoclast differentiation. Blood 106: 852-859, 2005.
35. Kim MS, Yang YM, Son A, Tian YS, Lee SI, Kang SW, Muallem S and Shin DM: RANKL-mediated reactive oxygen species pathway that induces long lasting Ca^{2+} oscillations essential for osteoclastogenesis. J Biol Chem 285: 6913-6921, 2010.
36. Ha H, Kwak HB, Lee SW, Jin HM, Kim HM, Kim HH and Lee ZH: Reactive oxygen species mediate RANK signaling in osteoclasts. Exp Cell Res 301: 119-127, 2004.
37. Bhatt NY, Kelley TW, Khramtsov VV, Wang Y, Lam GK, Clanton TL and Marsh CB: Macrophage-colony-stimulating factor-induced activation of extracellular-regulated kinase involves phosphatidylinositol 3-kinase and reactive oxygen species in human monocytes. J Immunol 169: 6427-6434, 2002.
38. Fan Z, Gao Y, Huang Z, Xue F, Wu S, Yang J, Zhu L and Fu L: Protective effect of hydrogen-rich saline on pressure overload-induced cardiac hypertrophyin rats: Possible role of JAK-STAT signaling. BMC Cardiovasc Disord 18: 32, 2018.
39. Chen Y, Jiang J, Miao H, Chen X, Sun X and Li Y: Hydrogen-rich saline attenuates vascular smooth muscle cell proliferation and neointimal hyperplasia by inhibiting reactive oxygen species production and inactivating the Ras-ERK1/2-MEK1/2 and Akt pathways. Int J Mol Med 31: 597-606, 2013.
40. Qiu X, Li H, Tang H, Jin Y, Li W, YuSun, PingFeng, Sun X and Xia Z: Hydrogen inhalation ameliorates lipopolysaccharide-induced acute lung injury in mice. Int Immunopharmacol 11, 2130-2137, 2011.
41. Wang K, Song X, Duan S, Fang W, Huan X, Cao Y, Tang J and Wang L: Hydrogen-rich saline prevents the down regulation of claudin-5 protein in septic rat lung via the PI3K/Akt signaling pathway. Int J Clin Exp Med 10: 11717-11727, 2017.
42. Zhang Y, Liu Y and Zhang J. Saturated hydrogen saline attenuates endotoxin-induced lung dysfunction. J Surg Res 198: 41-49, 2015.
43. Liu H, Liang X, Wang D, Zhang H, Liu L, Chen H, Li Y, Duan Q and Xie K: Combination therapy with nitric oxide and molecular hydrogen in a murine model of acute lung injury. Shock 43: 504-511, 2015.
44. Takayanagi H, Kim S, Matsuo K, Suzuki H, Suzuki T, Sato K, Yokochi T, Oda H, Nakamura K, Ida N, *et al*: RANKL maintains bone homeostasis through c-Fos-dependent induction of interferon-β. Nature 416: 744-749, 2002.
45. Grigoriadis AE, Wang ZQ, Cecchini MG, Hofstetter W, Felix R, Fleisch HA and Wagner EF: c-Fos: A key regulator of osteoclast-macrophage lineage determination and bone remodeling. Science 266: 443-448, 1994.
46. Jiao Z, Xu W, Zheng J, Shen P, Qin A, Zhang S and Yang C: Kaempferide prevents titanium particle induced osteolysis by suppressing JNK activation during osteoclast formation. Sci Rep 7: 16665, 2017.